

# 3-D Pushover Analysis for Damage Assessment of Buildings

A.S. Moghadam<sup>1</sup> and W.K. Tso<sup>2</sup>

1. Assistant Professor, Structural Engineering Research Center, International Institute of Earthquake Engineering and Seismology (IIEES), P.O. Box 19395-3913, Tehran, Iran, email: Moghadam@dena.iiees.ac.ir
2. Professor, Civil Engineering Department, McMaster University, Hamilton, Ontario, L8S 4L7, Canada, email: Tsowk@mcmaster.ca

**ABSTRACT:** *The Pushover procedure is extended for seismic damage assessment of asymmetrical buildings. By mean of an example, it is shown that the accuracy of the proposed 3-D pushover analysis is similar to those applied to planar structures. The procedure is found to be more successful in estimating the global response parameters such as interstorey drifts than local damage indicators such as beam or column ductility demands.*

**Keywords:** Pushover analysis; Nonlinear analysis; Dynamic analysis, Multistorey building; 3-D analysis

## 1. Introduction

Recent interests in the development of performance based codes for the design or rehabilitation of buildings in seismic active areas show that an inelastic procedure commonly referred to as the pushover analysis is a viable method to assess damage vulnerability of buildings [1, 9]. In brief, a pushover analysis is a series of incremental static analyses carried out to develop a capacity curve for the building. Based on the capacity curve, a target displacement which is an estimate of the displacement that the design earthquake will produce on the building is determined. The extent of damage experienced by the building at this target displacement is considered representative of the damage experienced by the building when subjected to design level ground shaking.

This approach has been developed by many researchers [3, 4, 7, 8], with minor variation in computation procedure. In most studies, the method was applied to symmetrical structures. Assuming the floors act as rigid diaphragms, the state of damage of the building can be inferred from applying a two dimensional pushover analysis on the building. If all the lateral load-resisting elements are similar, one can further simplify the problem to perform pushover analyses on a typical element of the building. The advantages and the limitations of 2D pushover analyses for damage assessment are described by Lawson et al [5]. One limitation is that the method does not account for the three-dimensional effect [9].

This paper extends the pushover analysis to cover plan-eccentric buildings and take the three-dimensional torsional effect into account. Because of torsional deformation, floor displacements of the building will consist of both translational and rotational components. The lateral load resisting elements located at different

positions in plan will experience different deformations. Torsional effect can be particularly damaging to elements located at or near the flexible edge of the building where the translational and rotational components of the floor displacement are additive. In view of the damage observed in many eccentric buildings in past earthquakes, it is the purpose of the present study to extend the 2-D pushover analysis procedure so that the vulnerability of elements located near the flexible edge of plan-eccentric buildings can be assessed.

## 2. Procedure

The procedure in the 3-D pushover analysis follows similar steps used in the two dimensional pushover analysis. First, the capacity curve is obtained by performing a series of three dimensional static analyses on the building when it is subjected to a set of forces  $V\{f\}$  applied at the centres of mass (CM) of the floors of the building.  $V$  represents the base shear and  $\{f\}$  is the normalised load vector. The capacity curve is given by the  $V$ - $\Delta$  relation obtained from the static analyses where  $\Delta$  is the CM displacement at the roof. Since the CM of the floors may not coincide with the centres of rigidity (CR) of the floors, the CM roof displacement would reflect both the translational and torsional deformation of the building under seismic lateral loading. The capacity curve has an initial linear range with a slope  $k$ , and can be expressed in the form  $V = k \times G(\Delta)$  where  $G(\Delta)$  is a function describing the shape of the capacity curve. An equivalent single degree of freedom (SDOF) system can be established to obtain the target displacement as follows:

The equation of motion for a N-storey building subjected to horizontal ground motion  $\ddot{u}_g$  in one direction

(the y-direction) can be written as

$$\begin{bmatrix} [m_x] & [0] & [0] \\ [0] & [m_y] & [0] \\ [0] & [0] & [I_m] \end{bmatrix} \{\ddot{u}\} + \{R\} = - \begin{bmatrix} [m_x] & [0] & [0] \\ [0] & [m_y] & [0] \\ [0] & [0] & [I_m] \end{bmatrix} \ddot{u}_g(t) \quad (1)$$

in which

$[m_x], [m_y]$  and  $[I_m]$ : the mass matrix in x and y-direction and mass moment of inertia matrix about CM

$\{u\} = \text{col}(\{u_x\}, \{u_y\} \text{ and } \{\theta\})$

$\{u_x\}, \{u_y\}$ : x and y-direction displacement vector referred to the centres of mass (CM) of the floors

$\{\theta\}$ : the floor rotation vector

$\{R\}$ : the restoring force vector

Assuming a single mode response, the displacement vector  $\{u\}$  can be written as

$$\{u\} = \begin{Bmatrix} \{\phi_x\} \\ \{\phi_y\} \\ \{\phi_\theta\} \end{Bmatrix} \Delta(t) = \{\phi\} \Delta(t) \quad (2)$$

where  $\Delta(t)$  is the generalised coordinate, representing the CM roof displacement, and  $\{\phi\}$  is an assumed deformation profile for the building. Further, the restoring force vector  $\{R\}$  is approximately represented by the y-direction pushover analysis and can be written as

$$\{R\} = k \times G(\Delta) \begin{Bmatrix} \{0\} \\ \{f\} \\ \{0\} \end{Bmatrix} \quad (3)$$

Using relations (2) and (3), the equation of motion for the generalised coordinate  $\Delta(t)$  can be obtained from Eq. (1) as

$$m^* \ddot{\Delta} + k^* G(\Delta) = -L^* \ddot{u}_g(t) \quad (4)$$

where

$$m^* = \text{generalised mass} \equiv \{\phi\}^T \begin{bmatrix} [m_x] & [0] & [0] \\ [0] & [m_y] & [0] \\ [0] & [0] & [I_m] \end{bmatrix} \{\phi\}$$

$$k^* = \text{generalised stiffness} \equiv k \{\phi\}^T \begin{Bmatrix} \{0\} \\ \{f\} \\ \{0\} \end{Bmatrix}$$

$L^* = \text{generalised earthquake excitation factor}$

$$\equiv \{\phi\}^T \begin{bmatrix} [m_x] & [0] & [0] \\ [0] & [m_y] & [0] \\ [0] & [0] & [I_m] \end{bmatrix} \begin{Bmatrix} \{0\} \\ \{1\} \\ \{0\} \end{Bmatrix}$$

The effect of damping is introduced directly at this stage as a viscous damping term  $c^* \times \dot{\Delta}$ , in which  $c^* = 2\xi \omega^* m^*$ ,  $(\omega^*)^2 = k^*/m^*$  and  $\xi = \text{damping ratio}$ ; leading to the final equation

$$m^* \ddot{\Delta} + c^* \dot{\Delta} + k^* G(\Delta) = -L^* \ddot{u}_g(t) \quad (5)$$

For a given excitation  $\ddot{u}_g$ , the solution of Eq. (5) is obtained using a step by step integration procedure and the absolute maximum of  $\Delta(t)$ , denoted by  $\Delta_{max}$  is a predictor of the maximum CM displacement at the roof of the structure. Once,  $\Delta_{max}$  is determined, a second 3-D pushover analysis will be carried out. The second pushover analysis terminates when the CM displacement at the roof of the structure equals to  $\Delta_{max}$ . The deformation and damage on elements near the flexible edge of the building at this stage of the pushover analysis would then be taken as indicative of the deformation and damage of these elements in the building when the building is subjected to the earthquake ground shaking.

### 3. Example Buildings

A seismic damage assessment is performed on two uniform seven-storey reinforced concrete buildings to illustrate the procedure. Building S is symmetric and Building A is plan-eccentric. Each building has a rectangular plan measuring 24m by 17m. The lateral load resisting elements in the y-direction consist of three identical ductile moment resisting frames. Frame 2 is located at the geometric centre of the plan and frames 1 and 3 are located at equal distance, but opposite side of frame 2. The spacing between frames are 9m, as shown in Figure (1a). For simplicity, the x axis is taken as an axis of symmetry and it is assumed that the x-direction lateral load resisting elements are located along the x axis so that they will not contribute to resist excitations in the y-direction. In building S, the floor masses are uniformly distributed so that the CM of each floor coincides with the geometric centre. In building A, the mass distribution of each floor causes the CM of the floor to shift a distance of 2.4m from frame 2 towards frame 3. Therefore, building A is mass eccentric, and has a constant floor eccentricity equal to 10% of plan dimension. The right hand edge of this building is the flexible edge, susceptible to large additional displacement, while frame 3 is the frame that is most vulnerable in terms of ductility demands.

The buildings are designed for 0.3g effective peak acceleration, using a design spectrum that has a shape similar to the Newmark-Hall 5% damped average spectrum. The strength of the buildings is designed based on a base shear value equal to 15% of the elastic base shear so that when exposed to ground motions of design intensity, the buildings will be excited well into the inelastic range. The design base shear equals to 1200kN. Each frame is designed to take one third of the design base shear. Each

frame has three bays and uniform storey height of 3m, as shown in Figure (1b). The strength of the beams and columns in the frame are allocated following the “strong column-weak beam” capacity design procedure. No torsional provisions are taken into account in the design of each frame. The properties of frame are given in the Appendix. The fundamental periods of building S and building A are 1.35 second and 1.52 second respectively.

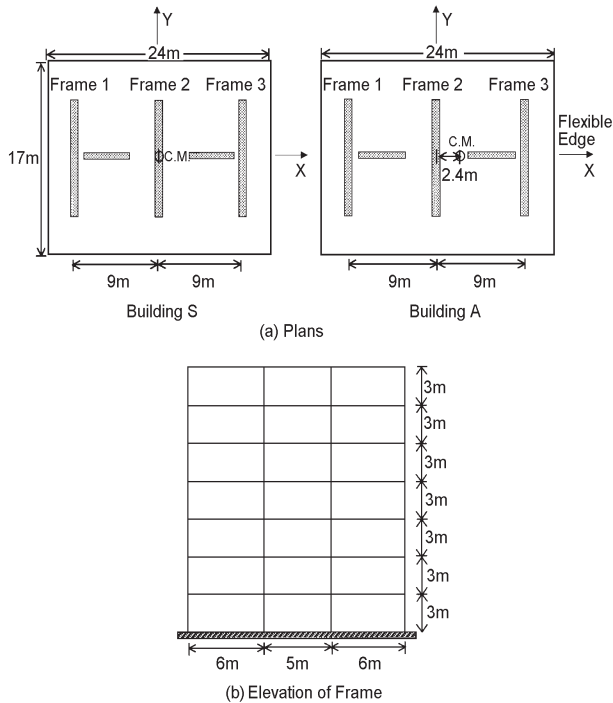


Figure 1. Example buildings.

The inclusion of building S in this study serves two purposes. First, a comparison of the seismic responses at the flexible edge, and also at frame 3 of both buildings A and S will show the torsional effect on the displacements and ductility demands at the critical edges of multi-storey buildings with eccentric plans. Since all frames are identical, no load redistribution among frames will occur in building S. The results obtained from the pushover analysis on building S is identical to those if a 2-D pushover analysis were performed on a typical frame. A comparison of the accuracy of the pushover results on both buildings A and S will therefore provide a measure of the accuracy of the 3-D pushover procedure. The accuracy of the pushover results on both buildings were established by making comparison to results obtained using inelastic dynamic analyses on the buildings, treating them as multi-degrees of freedom (MDOF) systems. Both the 3-D pushover analyses and inelastic dynamic analyses were carried out using the computer code CANNY [6].

4. Ground Motion Input

Since inelastic responses can be sensitive to the actual waveform of a single earthquake record, an ensemble of ten horizontal ground motion records was used as input.

Each record was normalised to a peak ground acceleration of 0.3g. The records were chosen based on the criterion that the shape of their response spectra being similar to that of the design spectrum. The mean and mean plus one standard deviation of the 5% damped acceleration response spectra for the ensemble of records, and also the corresponding Newmark-Hall spectra, are shown in Figure (2). The list of records used is presented in Table (1).

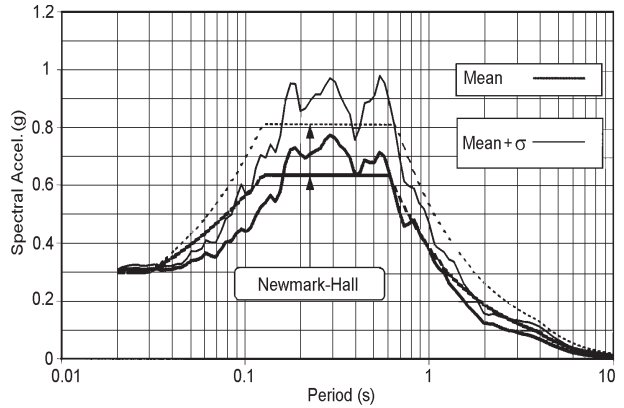


Figure 2. Response spectrum for 10 records.

5. Results

To obtain the capacity curve, a triangular distribution of the forces along the height of the building was assumed. The resulting capacity curves for the two buildings are shown in Figure (3). Both curves show similar features. They are linear initially but start to deviate from linearity when inelastic actions start to take place in the beams and later in the columns. When the buildings are pushed well into the inelastic range, the capacity curves again become essentially linear, but with a much smaller slope. Both curves can be approximated by means of a bilinear relationship, as shown in the figure. The curve associated with building A is less stiff, and yields at a lower base shear value than that of building S. This can be expected as the CM roof displacement of building A takes into account both the translational and torsional deformation of the building. Four stages of building deformation marked 1, 2, 3, and 4 are shown in the same figure. Stage 1 can be considered as the stage when the buildings begin to yield

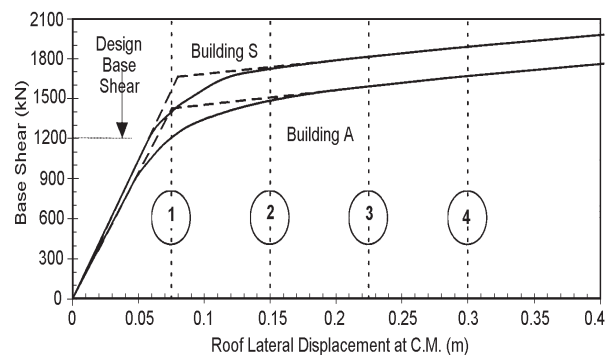


Figure 3. The performance curves for buildings A and S.

Table 1. List of earthquake records.

Earthquake Site	Date	Mag.	Soil	Source Dist. (km)	Y Comp.	X Comp.
Imperial Valley, California <i>El Centro</i>	05/18/40	6.6	Stiff Soil	8	S00E	S90W
Kern County, California <i>Taft Lincoln School Tunnel</i>	07/21/52	7.6	Rock	56	S69E	N21E
San Fernando, California <i>Hollywood Storage PE. Lot, LA</i>	02/09/71	6.6	Stiff Soil	35	N90E	S00W
San Fernando, California <i>Griffith Park Observatory, LA</i>	02/09/71	6.6	Rock	31	S00W	S90W
San Fernando, California <i>234 Figueroa St., LA</i>	02/09/71	6.6	Stiff Soil	41	N37E	S53E
Near S. Coast of Honshu, Japan <i>Kushiro Central Wharf</i>	08/02/71	7.0	Stiff Soil	196	N90E	N00E
Near E. Coast of Honshu, Japan <i>Kashima Harbor Works</i>	11/16/74	6.1	Stiff Soil	38	N00E	N90E
Monte Negro, Yugoslavia <i>Albatros Hotel, Ulcinj</i>	04/15/79	7.0	Rock	17	N00E	N90W
Michanocan, Mexico <i>El Suchil, Guerrero Array</i>	09/19/85	8.1	Rock	230	S00E	N90W
Michanocan, Mexico <i>La Villita, Guerrero Array</i>	09/19/85	8.1	Rock	44	N90E	N00E

in an overall sense. Stages 2, 3 and 4 correspond to buildings being displaced to 2 times, 3 times and 4 times the overall yield displacement respectively.

The displacements and interstorey drift ratios at the right hand edge of the buildings are compared at different stages of building deformation. Shown in Figure (4) are the floor displacement profiles for both buildings. For a given stage, the edge displacements of building A is larger than those of building S, since the torsional displacements are additive to the translational displacements at this edge in building A. Of more interest to damage assessment is the interstorey drift ratio which are shown in Figure (5). The actual drift ratios differ significantly between the two

buildings. For the same stage of building deformation, the maximum interstorey drift ratio of building A is about 60% above that of building S.

To reduce the 3N degrees of freedom system describing the building to the equivalent SDOF system, a constant deformation profile at CM of the building is needed. Shown in Figure (6) are the normalised displacement profiles at CM and also at the flexible edge of building A for the four stages of building deformation. It appears that the normalised displacement profiles are not sensitive to the stages of building deformation. A displacement profile at any deformation stage is a suitable profile to be used in Eq. (2). To be specific, the suggestion

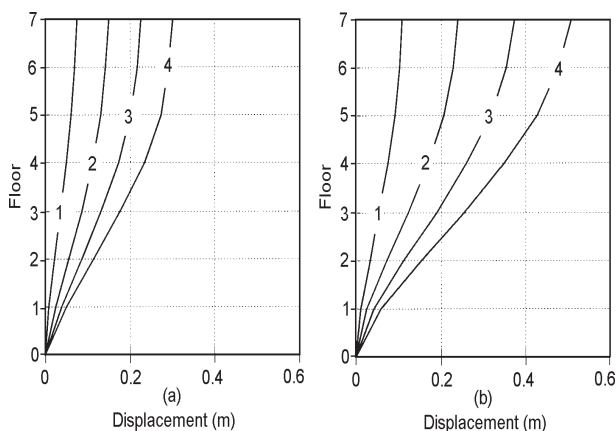


Figure 4. Floor displacement at edge 3 (a) building S (b) building A.

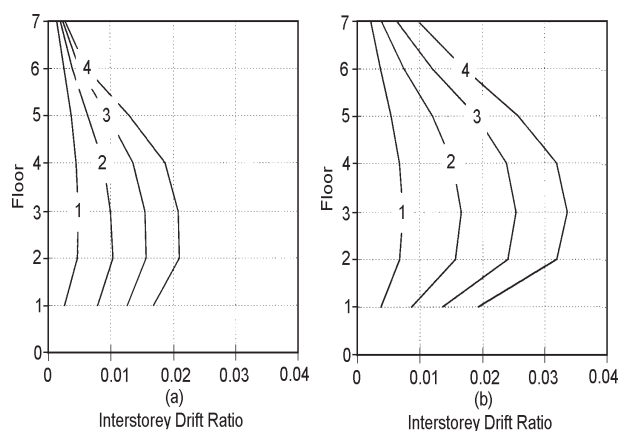


Figure 5. Interstorey drift ratio at edge 3 (a) building S (b) building A.

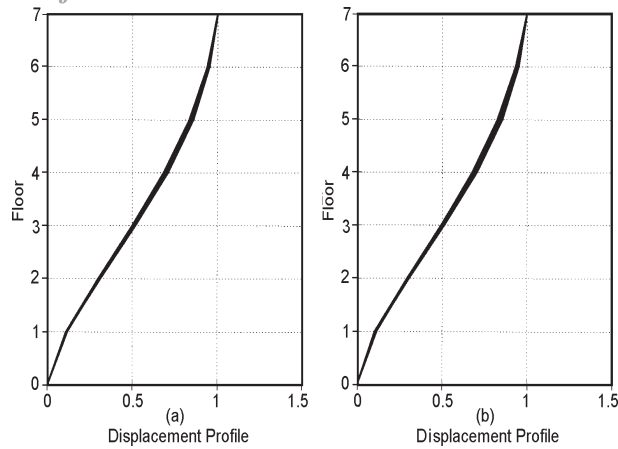


Figure 6. Displacement profile of building A (a) at CM, (b) at edge 3.

of Qi and Moehle [7] using the deformation profile when the top CM displacement equals to 1% of the total height was adopted in creating the equivalent SDOF system in this study.

Three types of responses at or near the flexible edge are of interest in the damage assessment process. They are

- (i) The seismic displacements for non-structural damage assessment,
- (ii) Ductility demands for member damage assessment, and
- (iii) Period changes for overall building damage assessment.

5.1. Seismic Displacements

Shown in Figure (7) is the correlation diagram of the maximum roof CM displacement of the building, computed based on inelastic dynamic analyses of the equivalent SDOF system and the MDOF system. The solid diagonal line denotes perfect correlation and the dotted lines provide the plus and minus 25% bound of the correlation. Each point on the plot corresponds to the response of a building to one scaled earthquake record input. The open squares represent responses from building S, and the solid

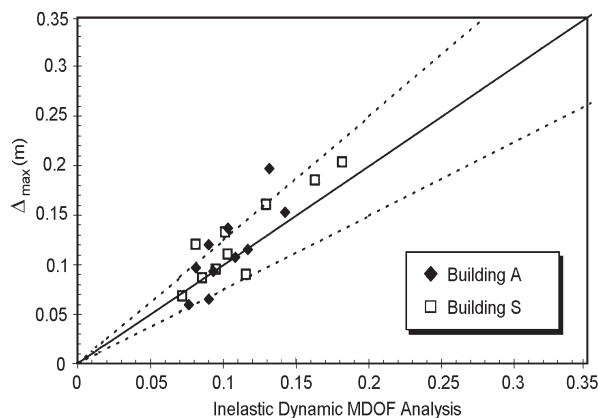


Figure 7. Maximum roof CM displacement (meter).

diamonds denote responses from building A. Two observations can be made. First, the scatter of the results from building A and building S is similar. Second, one can expect accuracy in the order of plus or minus 25% using the proposed procedure to estimate the seismic CM displacement at the roof of the building.

The correlation for the maximum top displacement and maximum interstorey drift ratio at the flexible edge of the buildings are shown in Figures (8) and (9). Again, the plots show that the procedure is capable of estimating these two quantities within 25% accuracy. There is in general a segregation of the results from the two buildings, with large maximum top displacement and also larger maximum interstorey drift ratio from building A. This trend can be expected due to the eccentric nature of building A.

Another way to assess the accuracy of the procedure to estimate seismic displacement quantities at or near the flexible edge is to carry out a statistical analysis and focus on the mean and mean plus one standard deviation comparisons. Shown in Figure (10) is the comparison of the mean of the maximum floor displacements for buildings S and A. Within each plot, the solid line represents the prediction from the proposed procedure, using the mean of  $\Delta_{max}$  as the seismic displacement target in the 3D pushover analysis. The points are the

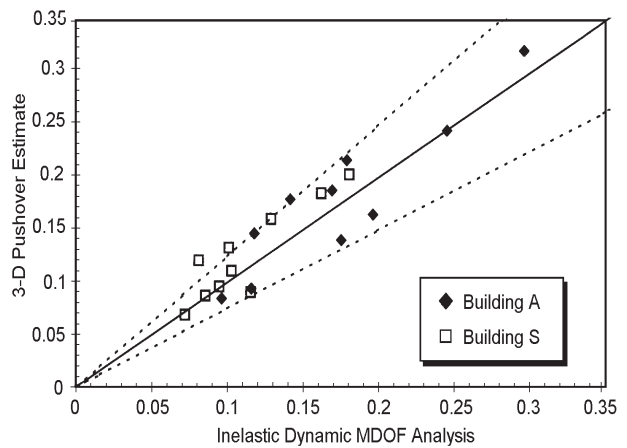


Figure 8. Maximum top displacement at edge 3 (unit in meter).

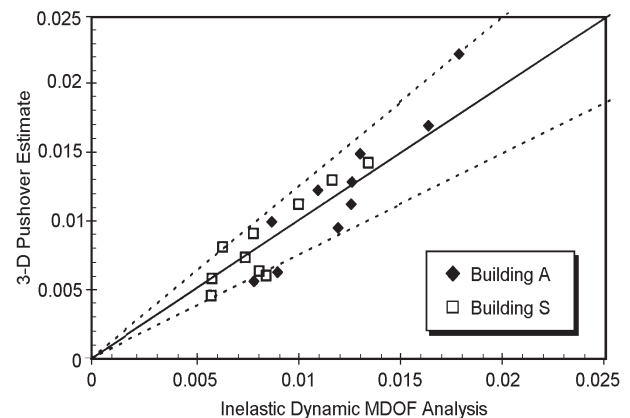


Figure 9. Maximum interstorey drift ratio at edge 3.

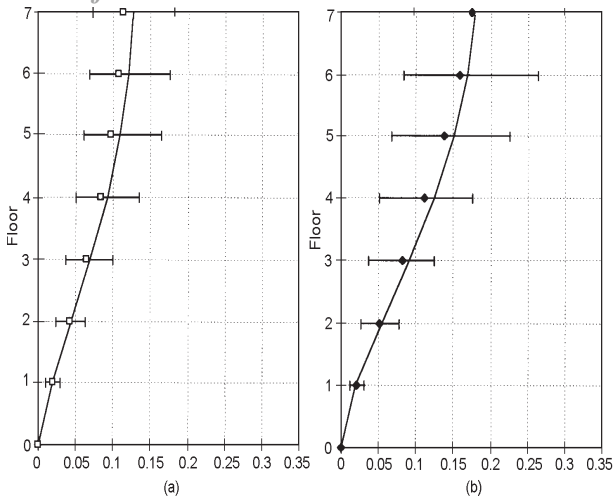


Figure 10. Pushover estimation (mean) of maximum displacements at edge 3 (meter) (a) building S (b) building A.

mean of the maximum floor displacements based on inelastic dynamic MDOF analyses. For each floor, a bar graph is also included to denote the range of maximum floor displacement values experienced by the building under the ensemble of earthquake records used. Shown in Figure (11) is a similar comparison on the mean plus one standard deviation estimation of the same quantity. To be consistent, the mean plus one standard deviation value for  $\Delta_{max}$  was used as the target seismic displacement in the 3D pushover analysis. It shows that the procedure leads to very good prediction of the maximum floor displacements in a statistical sense.

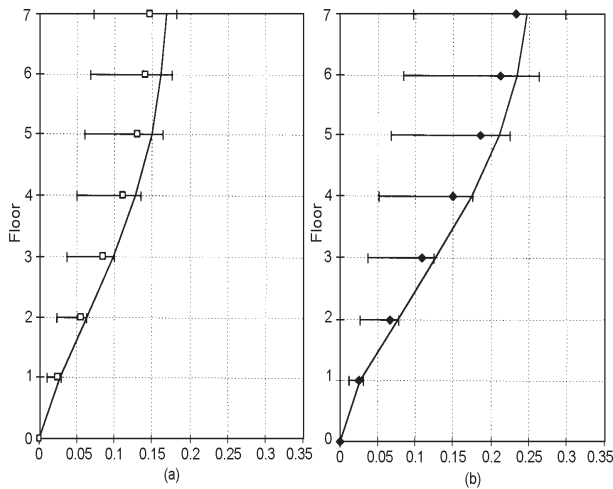


Figure 11. Pushover estimation (mean +  $\sigma$ ) of maximum displacements at edge 3 (meter) (a) building S (b) building A.

Similar comparisons are carried out on the prediction of the maximum interstorey drift ratios at the flexible edge along the height of the buildings. The results are presented in Figures (12) and (13). The comparison shows that the procedure predicts well the interstorey drift ratio for floors from ground up to the mid-height of the building where the interstorey drift ratio is the largest. However, the pushover analysis tends to underestimate the interstorey

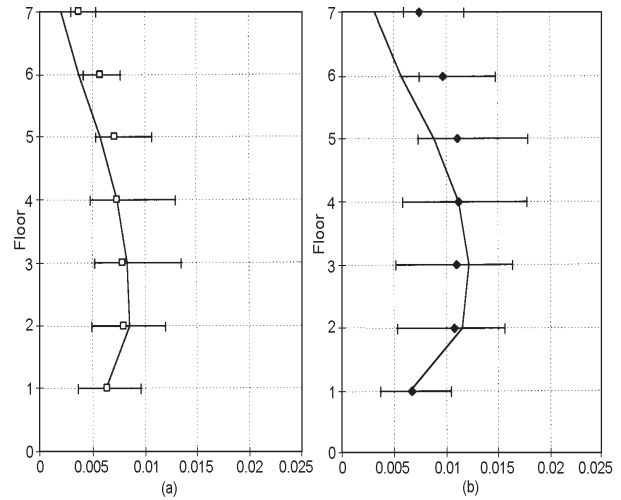


Figure 12. Pushover estimation (mean) of maximum interstorey drift ratio at edge 3 (a) building S (b) building A.

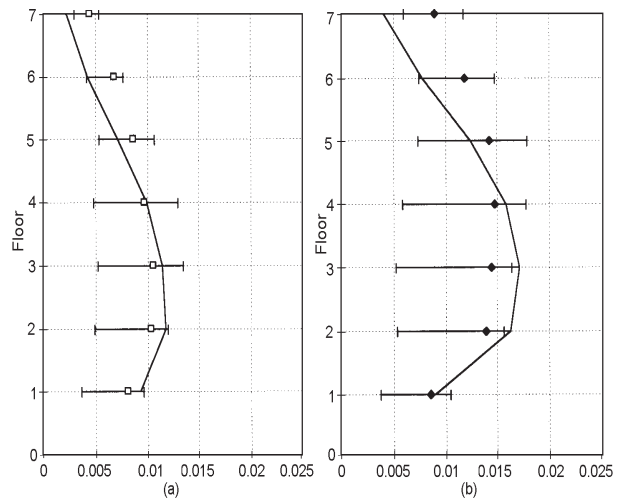


Figure 13. Pushover estimation (mean +  $\sigma$ ) of maximum interstorey drift ratio at edge 3 (a) building S (b) building A.

drifts at the upper floors. Higher modal contributions may be the cause of this underestimation.

### 5.2. Ductility Demands

To assess the member damage, the maximum ductility demands on the beams and columns are considered. The correlation diagrams for the maximum ductility demands of the beams and also columns for the two buildings are presented in Figures (14) and (15) respectively.

The ability of the procedure to predict local damages to members is not as good as predicting seismic displacements. A number of points lie outside the plus and minus 25% bounds. The trend shows that the pushover analysis underestimates the ductility demands, both of beams and columns for a number of earthquake records used.

A comparison for the pushover estimate to predict the mean maximum ductility demands of beams and columns in frame 3 are shown in Figures (16) and (17). It shows that the pushover analysis leads to a reasonable estimate of

the mean beam ductility demands in floors from the ground up to the middle of the building, but it underestimates the demands in the upper floors. The pushover analysis underestimates the mean column ductility demands in both buildings.

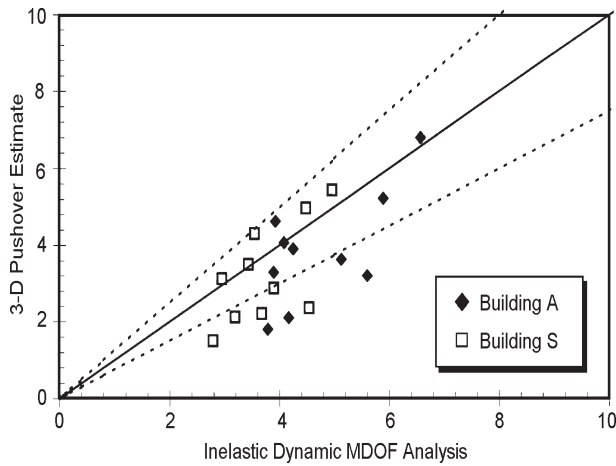


Figure 14. Maximum ductility demand of beams on Frame 3.

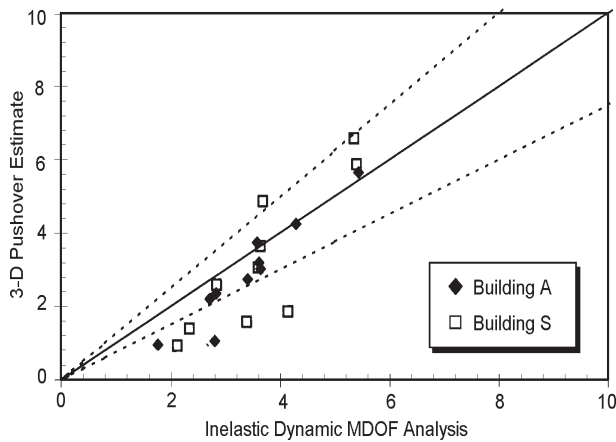


Figure 15. Maximum ductility demand of columns on Frame 3.

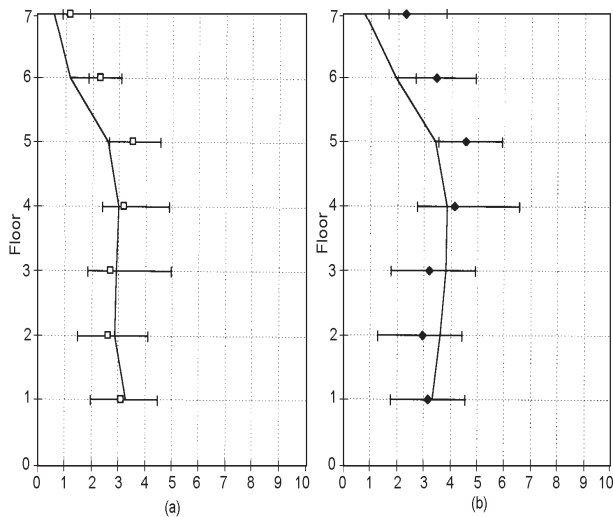


Figure 16. Pushover estimation (mean) of maximum ductility demand in beams on Frame 3; (a) building S (b) building A.

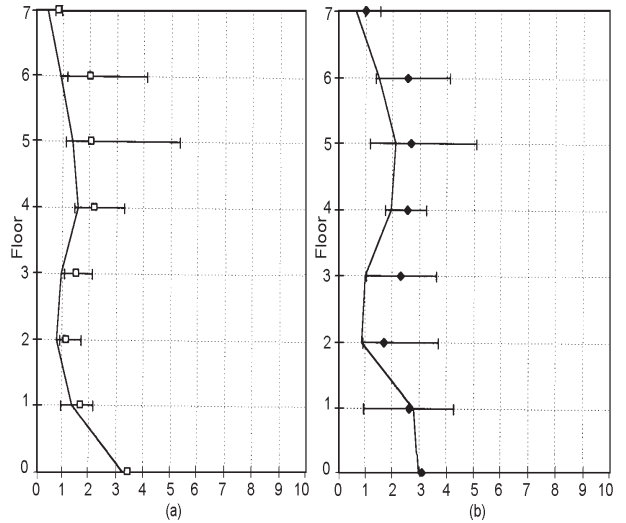


Figure 17. Pushover estimation (mean) of maximum ductility demand in columns of Frame 3; (a) building S (b) building A.

### 5.3. Period Changes

One of the useful parameters for global damage assessments is the change in fundamental period of the building. The fundamental period changes when the building is excited into the inelastic range. The variation of the fundamental period of the building with time for one of the earthquake excitation is shown in Figure (18). The duration when the period exceeds the elastic period  $(T_1)_0$  corresponds to the building being excited into the inelastic range. The maximum change of the period can conveniently be denoted by the period ratio which is defined as the maximum period divided by the elastic period of the building. Once the period ratio is known one can compute the maximum softening index which is considered the best indicator of the global damage state [10]. One can also compute a period ratio based on the pushover analysis by determining the period of the building at the beginning and at the end of the pushover analysis. A correlation between the period ratio as determined by 3D inelastic

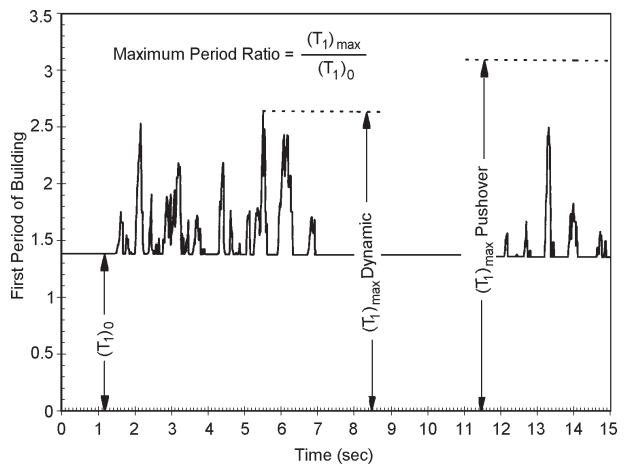


Figure 18. Change in period during earthquake.

## Archive of SID

dynamic MDOF analysis and pushover analysis will provide an indication on how well the proposed procedure can assess the global damage of the building. The correlation diagram for maximum period ratio for the two buildings is shown in Figure (19). It shows that the pushover analysis generally overestimates the period ratio. This trend can be expected since there is no unloading during the pushover analysis. The degree of correlation shown in the figure is similar to that for estimating the maximum interstorey drift ratio, namely most points lies within the plus or minus 25% bounds.

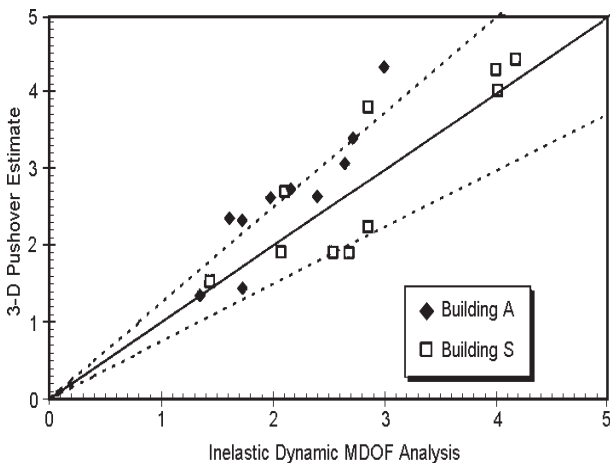


Figure 19. Maximum period ratio correlation.

## 6. Conclusions

In this paper, the use of the pushover analysis to assess seismic damage to buildings has been extended to include the three dimensional effect of building responses. This extension has enlarged the scope of pushover analysis to include plan-eccentric buildings which are very susceptible to seismic damages. By means of examples, it is shown that

- (i) The accuracy of the proposed 3-D pushover analysis, for the buildings used here, is similar to that of the currently used pushover analysis method for planar structures;
- (ii) The pushover analysis procedure is more successful to predict global response parameters such as edge displacements, interstorey drift ratios, and fundamental period changes than local damage parameters such as member ductility demands;
- (iii) The seismic demands at or near the flexible edge of plan-eccentric buildings are higher due to the torsional effect.

It is worthwhile to mention a limitation of the proposed 3-D pushover analysis method. For plan-eccentric buildings, the vibration modes are coupled modes consisting of both translational and torsional motions. Since the procedure assumes that the building responds mainly in its fundamental mode, it would give

representative results when the fundamental mode of the building is translation predominate. For torsionally flexible buildings, the fundamental mode is torsion predominant and more than one mode will contribute significantly to the overall responses. The dynamic behavior of this class of eccentric buildings would violate the basic assumptions of the pushover analysis method.

Further research is needed to check the accuracy of 3-D pushover procedure when the building is asymmetric in respect to both axes and subjected to simultaneous ground motion in both directions.

## Acknowledgment

The writers wish to acknowledge the support of the Natural Sciences and Engineering Research Council of Canada (NSERC) and the International Institute of Earthquake Engineering and Seismology (IIEES) for the work presented.

## References

1. ATC (1995). "Guidelines for the Seismic Rehabilitation of Buildings", *ATC 33.03*, Applied Technology Council, Redwood City, California.
2. Collins, K.R. (1995). "A Reliability-Based Dual Level Seismic Design Procedure for Building Structures", *Earthquake Spectra*, **11**, 417-429.
3. Fajfar, P. and Fischinger, M. (1988). "N2-A Method for Non-Linear Seismic Analysis of Regular Buildings", *Proc. 9<sup>th</sup> World Conference on Earthquake Engineering*, Tokyo, **5**, 111-116.
4. Fajfar, P. and Gasperisic, P. (1996). "The N2 Method for the Seismic Damage Analysis of RC Buildings", *J. Earthquake Engineering and Structural Dynamics*, **25**, 31-46.
5. Lawson, R.S, Vance, V., and Krawinkler, H. (1994). "Nonlinear Static Pushover Analysis Why, When and How?", *5<sup>th</sup> U.S. National Conference on Earthquake Engineering*, Chicago, Illinois, **1**, 283-292.
6. Li, K-N. (1993). "CANNY-C: A Computer Program for 3D Nonlinear Dynamic Analysis of Building Structures", Research Report No. CE004, National University of Singapore.
7. Qi, X. and Moehle, J.P. (1991). "Displacement Design Approach for Reinforced Concrete Structures Subjected to Earthquakes", Report UCB/EERC-91/02, Earthquake Engineering Research Center, University of California-Berkeley.
8. Saidii, M. and Sozen, M. (1981). "Simple Nonlinear Seismic Analysis of R/C Structures", *J. Struct. Div., ASCE*, **107**, 937-952.



9. Vision 2000 (1995). "Performance Based Seismic Engineering of Buildings", Structural Engineers Association of California, Sacramento, California.
10. Williams, M.S. and Sexsmith, R.G. (1995). "Seismic Damage Indices for Concrete Structures: A State-of-the-Art Review", *Earthquake Spectra*, **11**(2), 319-349.

### Appendix

Data for typical frame of buildings S and A

Notes:

- Units are: Kilo Newton (kN) for force and meter for length
- All the section rigidities and strengths mentioned below for beams and columns are for bending. Some other rigidities are included in analyses, but in general they do not have much effect. They are
  - For beams: (elastic) shear rigidity of 3120826
  - For columns: (elastic) shear rigidity of 2902500
  - For columns: (elastic) axial rigidity of 6750000
  - For columns: (elastic) torsional rigidity of 120941.4
- The bending (flexural) behaviour of all beams and columns are modelled using bilinear curves with rigidities (EI) and strengths mentioned below and by including 3% hardening.

### Beams

Floor	EI	+Ve Strength	-Ve Strength
1	52920	246.33	-152.17
2	52920	279.77	-188.25
3	52920	267.52	-174.3
4	52920	238.49	-142.72
5	52920	199.25	-117.11
6	52920	156.61	-117.11
7	52920	117.11	-117.11

### Exterior Columns

Storey	EI	+Ve Strength	-Ve Strength
1-bottom	98550	296.76	-296.76
1-top	98550	224.46	-224.64
2-bottom	98550	219.4	-219.4
2-top	98550	219.4	-219.4
3-bottom	98550	214.11	-214.11
3-top	98550	214.11	-214.11
4-bottom	98550	208.8	-208.8
4-top	98550	208.8	-208.8
5-bottom	98550	203.47	-203.47
5-top	98550	203.47	-203.47
6-bottom	98550	198.13	-198.13
6-top	98550	198.13	-198.13
7-bottom	98550	192.75	-192.75
7-top	98550	192.75	-192.75

### Interior Columns

Storey	EI	+Ve Strength	-Ve Strength
1-bottom	98550	317.73	-317.73
1-top	98550	270.93	-270.93
2-bottom	98550	261.59	-261.59
2-top	98550	300.32	-300.32
3-bottom	98550	292.03	-292.03
3-top	98550	274.28	-274.28
4-bottom	98550	265.56	-265.56
4-top	98550	230.57	-230.57
5-bottom	98550	221.01	-221.01
5-top	98550	216.53	-216.53
6-bottom	98550	206.87	-206.87
6-top	98550	206.87	-206.87
7-bottom	98550	197.25	-197.25
7-top	98550	247.7	-247.7